

# Upper-limit on the Advanced Virgo output mode cleaner cavity length noise

R Bonnard, M Ducrot, R Gouaty, F Marion, A Masserot,  
B Mours, E Pacaud, L Rolland, M Was

Laboratoire d'Annecy-le-Vieux de Physique des Particules (LAPP), Université  
Savoie Mont Blanc, CNRS/IN2P3, F-74941 Annecy, France

E-mail: [michel.was@lapp.in2p3.fr](mailto:michel.was@lapp.in2p3.fr)

**Abstract.** The Advanced Virgo detector uses two monolithic optical cavities at its output port to suppress higher order modes and radio frequency sidebands from the carrier light used for gravitational wave detection. These two cavities in series form the output mode cleaner. We present a measured upper limit on the length noise of these cavities that is consistent with the thermo-refractive noise prediction of  $8 \times 10^{-16}$  m/Hz<sup>1/2</sup> at 15 Hz. The cavity length is controlled using Peltier cells and piezo-electric actuators to maintain resonance on the incoming light. A length lock precision of  $3.5 \times 10^{-13}$  m is achieved. These two results are combined to demonstrate that the broadband length noise of the output mode cleaner in the 10-60 Hz band is at least a factor 10 below other expected noise sources in the Advanced Virgo detector design configuration.

PACS numbers: 04.80.Nn, 95.55.Ym

## 1. Introduction

Advanced interferometric gravitational wave detectors, such as Advanced Virgo [1], advanced LIGO [2], or GEO-HF [3] are making first detections or are about to start observations. All these detectors are using a special case of homodyne detection called DC readout [4, 5] to extract the differential arm length signal from the light at the interferometer output, that is the carrier light. A crucial element in the DC readout detection scheme is an output mode cleaner (OMC), which is a non-degenerate optical cavity that transmits only the fundamental Gaussian mode at the carrier frequency. The purpose is to keep only light which leaves the interferometer due to a gravitational wave signal and remove higher order modes caused by interferometer mirror defects and radio-frequency sidebands used for the control of auxiliary degrees of freedom.

One drawback of this scheme is that any length noise of the OMC cavity is imprinted on the transmitted light if the cavity length is not perfectly adjusted to the carrier frequency. The coupling factor is proportional to the root-mean-square of the difference between light carrier frequency and cavity resonant frequency.

A very low cavity length noise of a few  $10^{-17}$  m/Hz<sup>1/2</sup> at 1 Hz has been obtained for rigid cavities [6], however these have no means to tune the cavity length to follow the light frequency at the output of the interferometer. Although a scheme has been proposed to remove the need for cavity length actuator [7], all current detectors have actuators on the OMC length that may introduce additional length noise.

For advanced LIGO and GEO-HF the OMC is a 4-mirror bow-tie cavity with one of the mirrors directly mounted on a piezo-electric actuator (PZT) [2, 8], an upper limit of  $2 \times 10^{-14}$  m/Hz<sup>1/2</sup> on the cavity length noise introduced by this PZT has been measured in the 1-7 kHz band [8]. Advanced Virgo chose an alternative, more compact design with a single piece of fused silica forming a 4 surface bow-tie cavity [1] (see figure 1), based on previous experience from Virgo [9]. The cavity optical length can be controlled with two actuators, a Peltier cell that thermally changes the refractive index in the cavity and hence the optical length, and a PZT pressing the OMC transversely and allowing a fast control of the refractive index but with a low dynamic range. This choice should have the advantage of reducing noise from mechanical vibration and from the PZT, but has the drawback of light circulating in the substrate instead of vacuum, which among other things introduces additional thermal noise [10]. In order to obtain sufficient light filtering without introducing high thermal noise and large scattered light losses, two monolithic cavities are placed in series instead of a single cavity with high finesse.

In this paper we present an upper limit on the Advanced Virgo OMC length noise and the achieved precision of the OMC length control in a table top measurement. By combining these two measurements we derive the expected contribution of the OMC length noise to the Advanced Virgo measurement noise. In section 2 we discuss in detail the expected thermal length noise of the OMC and its coupling to the gravitational wave measurement, then in section 3 we describe the test measurement setup. Section 4 presents the length noise upper limit and section 5 the length control precision.

## 2. Advanced Virgo Output Mode Cleaner

The optimization of parameters for the Advanced Virgo OMC led to a design composed of two monolithic fused silica cavities in series [10], which allows good radio frequency

refractive index	$n$	1.44963
refractive index temperature dependence	$\beta$	$-10^{-5} \text{ K}^{-1}$
density	$D$	$2200 \text{ kg/m}^3$
thermal conductivity	$\kappa$	$1.38 \text{ Wm}^{-1}\text{K}^{-1}$
temperature	$T$	300 K
specific heat	$C$	$746 \text{ JK}^{-1}\text{kg}^{-1}$

**Table 1.** Fused silica parameters for thermo-refractive noise calculation (5)

filtering with low finesse and short cavities. Each OMC cavity is a single piece of fused silica with an elongated hexagon shape. The cavity has an effective length  $L = 0.124 \text{ m}$  (half of the round-trip length) which corresponds to an optical path length  $l_0 = nL$  where  $n$  is the fused silica refractive index. The cavity finesse was measured to be  $F \simeq 125$  and internal cavity losses at  $\sim 1.5\%$  [11]. One of the cavity surfaces is curved, with a radius of 1.7 m, and the beam resonating in the cavity has a waist  $w_0 = 321 \mu\text{m}$  located at the cavity input surface.

The cavity couples the fluctuations in optical path length  $l$  to power fluctuations  $\delta P$  of the transmitted light

$$\frac{\delta P}{P_0} = \frac{1}{1 + \left(\frac{2F}{\pi}\right)^2 \sin^2 \frac{2\pi l}{\lambda}} - 1, \quad (1)$$

where  $\lambda = 1064 \text{ nm}$  is the laser wavelength. In practice the optical path fluctuations are dominated by low frequency fluctuations, hence we decompose the cavity length fluctuations into a large dynamic, low frequency (below 10 Hz) component with root-mean-square (RMS)  $\Delta l_{\text{rms}}$  and a small component  $\delta l$  in the sensing band of Advanced Virgo (10 Hz–10 kHz)

$$l = l_0 + \Delta l_{\text{rms}} + \delta l. \quad (2)$$

Using this decomposition, (1) can be approximated above 10 Hz by

$$\frac{\delta P}{P_0} \simeq -32 F^2 \frac{\Delta l_{\text{rms}} \delta l}{\lambda^2}. \quad (3)$$

The corresponding noise on the gravitational wave signal is directly given by the power fluctuations in transmission of the OMC divided by interferometer response transfer function  $O_{\text{TF}}$ . Hence the OMC length noise coupling into the gravitational wave signal is

$$\delta h = -32 \sqrt{2} \frac{F^2 \Delta l_{\text{rms}} \delta l}{\lambda^2 O_{\text{TF}}}, \quad (4)$$

where the additional factor  $\sqrt{2}$  comes from adding in quadrature the length noise of the two OMC cavities, which is expected to be caused by statistical fluctuations in the substrate temperature and therefore independent.

Indeed, compared to a 4 mirror cavity design, a monolithic cavity has additional thermal fluctuations from the medium in which light circulates. Given that the thermal expansion coefficient of fused silica  $\alpha = 5 \times 10^{-7} \text{ K}^{-1}$  is small compared to the changes of the refractive index as a function of temperature  $\frac{dn}{dT} = \beta = -10^{-5} \text{ K}^{-1}$ , the dominant thermal length noise is thermo-refractive noise. There is also a contribution from Brownian noise and from all coatings thermal noises, but these are also negligible compared to thermo-refractive noise.

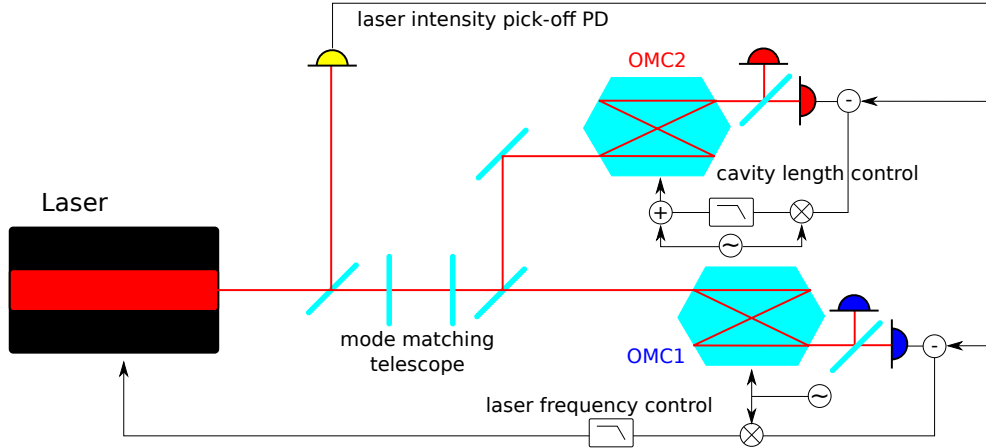


**Figure 1.** Schematic of the optical test setup (not to scale). The two OMC cavities OMC1 and OMC2 are set in parallel and each receives 45% of the laser beam, which in transmission of each cavity is split equally onto an in-loop and an out-of-loop PD. The flow of signal for the subtraction of laser intensity noise, the laser frequency control and the cavity length control is shown by arrows.

Thermo-refractive noise has been computed as a function of frequency  $f$  for an infinite plane of thickness  $L$  in appendix E of [12] and can be rewritten as

$$\delta l_{\text{thermo-refractive}}(f) \simeq \frac{2\beta T \sqrt{L k_B \kappa}}{DC \sqrt{\pi}} \frac{1}{(w_0/\sqrt{2})^2 2\pi f} \left[ \int_0^\infty \frac{x dx}{1 + \frac{4r_{\text{th}}^2}{w_0^2} x^2} e^{-x} \right]^{1/2}, \quad (5)$$

where  $k_B$  is the Boltzmann constant,  $r_{\text{th}} = \sqrt{\kappa/(2\pi f DC)}$  is the thermal path length,  $L = 0.124\text{m}$  is half of the cavity round-trip length and the values of the different parameters for fused silica are given in table 1. The integral term equates to 1 in the adiabatic limit where  $r_{\text{th}} \ll w_0$ . At low frequencies where  $r_{\text{th}} \gg w_0$ , the integral term is  $\propto f$ , hence the thermo-refractive noise remains bounded at low frequency. The transition between the two regimes occurs at  $f \sim 1.3\text{Hz}$  for the OMC cavity. The same result has been obtained more recently for a finite cavity of cylindrical geometry [13], which restrains its validity to the range where  $r_{\text{th}}$  is much larger than the wavelength and much smaller than the transverse size of the cavity (1 cm). This corresponds to a valid frequency range of 10 mHz–100 kHz, which covers well the frequency range of interest here. The principle of these computations has been confirmed by measuring thermo-refractive noise in a very different geometry of whispering-gallery mode of microspheres [14].

In section 4 we measure that the cavity length noise at 10 Hz is not larger than the one predicted by (5).

### 3. Experimental setup

The OMC cavity length fluctuations are measured using a dedicated optical test setup. The setup is located on a passively isolated optical bench, enclosed in aluminium and plexiglas covers placed on a tubular structure to prevent beam jitter from the clean room air flow. A schematic of the optical layout is shown on figure 1. A small

fraction (10%) of the light from a 2 W Mephisto laser [15] at 1064 nm is picked-off to a photo-diode (PD) to measure the laser intensity noise; the main part of the beam is matched with a telescope to two cavities set in parallel. This is different from the Advanced Virgo case where the two cavities are placed in series, and allows a simple measurement where light seen by one cavity is not directly affected by the other. For each cavity two PDs measure the transmitted power, which is between 30 mW and 80 mW depending on the PD.

To obtain an error signal for the cavity length, a dithering sine-wave, at a dozen kHz is applied to each cavity by a PZT. The cavity length error point is the PD signal demodulated at the dither frequency. This signal is limited by the laser intensity noise at the dither frequency. With the active power stabilization loop enabled (“noise eater” [15]), the laser intensity noise at a dozen kHz has a relative intensity  $\sim 2 \times 10^{-7} \text{ Hz}^{-1/2}$ . This laser intensity is measured by a pick-off PD and subtracted before demodulation.

The length error point is calibrated by scanning linearly the laser frequency over several cavity free spectral ranges, each free spectral range corresponding to a cavity length change of  $\lambda/2$ , as can be seen from (1). The measurement has an absolute statistical error of 2–3% and the systematic error from using the cavity length as a reference is less than 1%. Consequently the relative calibration is adjusted by several percent to obtain a good cancellation of common frequency noise between the two cavities. This cancellation is described in section 4.

#### 4. Cavity length noise measurement

In our measurement the laser frequency noise is dominant. Hence we lock the laser onto the length of OMC1 with a bandwidth of  $\sim 250 \text{ Hz}$  to reduce the frequency noise, and leave the OMC1 cavity length free. The OMC2 length is locked onto the laser frequency using Peltier cells and the PZT actuator with a loop unity gain frequency around 0.2 Hz.

Laser frequency noise  $\delta\nu$  couples to transmitted light fluctuation  $\delta P$  in the same way as cavity length noise as shown in (1). The spectra of the two cavities length error points are shown on figure 2 and are dominated by laser frequency noise. This frequency noise is equivalent to cavity length noise  $\delta l_{\text{laser}}$  using the relation

$$\frac{\delta\nu}{\nu} = -\frac{\delta\lambda}{\lambda} = \frac{\delta l_{\text{laser}}}{l_0}, \quad (6)$$

with  $\nu = 2.82 \times 10^{14} \text{ Hz}$  the light frequency. With this notation and dismissing other noise contributions the cavity calibrated error point can be written as

$$\text{EP}_{\text{OMC}} = \delta l_{\text{OMC}} + \delta l_{\text{laser}}. \quad (7)$$

Hence the difference between the two cavities

$$\text{EP}_{\text{diff}} = \text{EP}_{\text{OMC1}} - \text{EP}_{\text{OMC2}} = \delta l_{\text{OMC1}} - \delta l_{\text{OMC2}} \quad (8)$$

should be a good measure of the differential length, free of the common laser frequency noise. This is a true representation of the cavity differential length above 10 Hz as the OMC1 length is free and the OMC2 length control loop has a gain well below 1. However, some of the laser frequency noise is re-injected by PZT feedback of the OMC2 length control, as the loop gain at 10–100 Hz is  $\sim 0.02$  and not zero. This means that in addition to OMC2 free cavity length noise there is a loop feedback contribution  $\delta l_{\text{OMC2}} = \delta l_{\text{OMC2, free}} + \delta l_{\text{OMC2, PZT}}$ . The latter can be easily subtracted as the

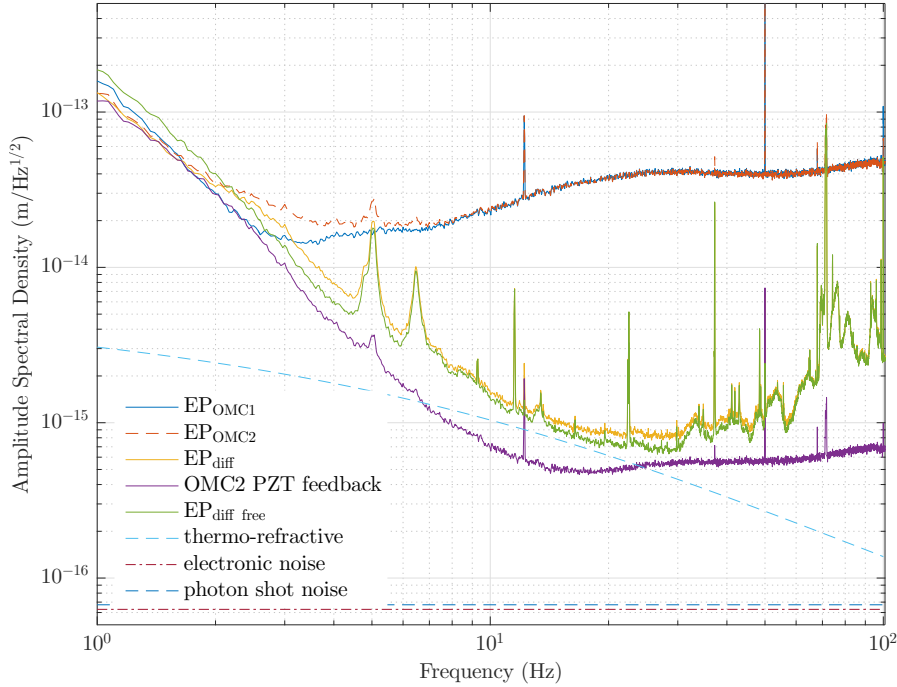


**Figure 2.** Differential OMC length noise measurement over 1.5 hours of data. Shown are the calibrated length error points for OMC1 and OMC2, their difference (8), and the difference with the OMC2 PZT feedback subtracted (9). For reference the expected thermo-refractive noise is shown along with electronic and photon shot noise.

feedback voltage is known and the cavity has a flat response of  $\chi = 2.6 \times 10^{-11}$  m/V at these frequencies, hence we define the loop corrected differential length as

$$EP_{\text{diff free}} = EP_{\text{OMC1}} - (EP_{\text{OMC2}} - \chi PZT_{\text{OMC2}}) = \delta l_{\text{OMC1,free}} - \delta l_{\text{OMC2,free}}. \quad (9)$$

These noise curves are shown on figure 2 averaged over 1.5 hours of data, and we have checked that this noise level is stationary at the few minutes time scale. Also shown are the PD electronic noise measured with the laser switched off and the expected photon shot-noise. For comparison the thermo-refractive noise of the two cavities from 5 added in quadrature is also shown. The measured cavity differential length shows many lines due to mechanical resonances of components on the optical bench, especially above 60 Hz the measurement is completely spoiled. At lower frequencies, the broad lines at 5 Hz and 6.5 Hz come from the tubular posts that hold plexiglas covers to prevent air-flow, and their coupling depends on the torque applied to the PZT clamping. Below 10 Hz there are large fluctuations that are not understood. Nonetheless in the 10-20 Hz band the measured noise is within 10% of the thermo-refractive prediction, and is an upper-limit that no length noise is larger than this prediction.

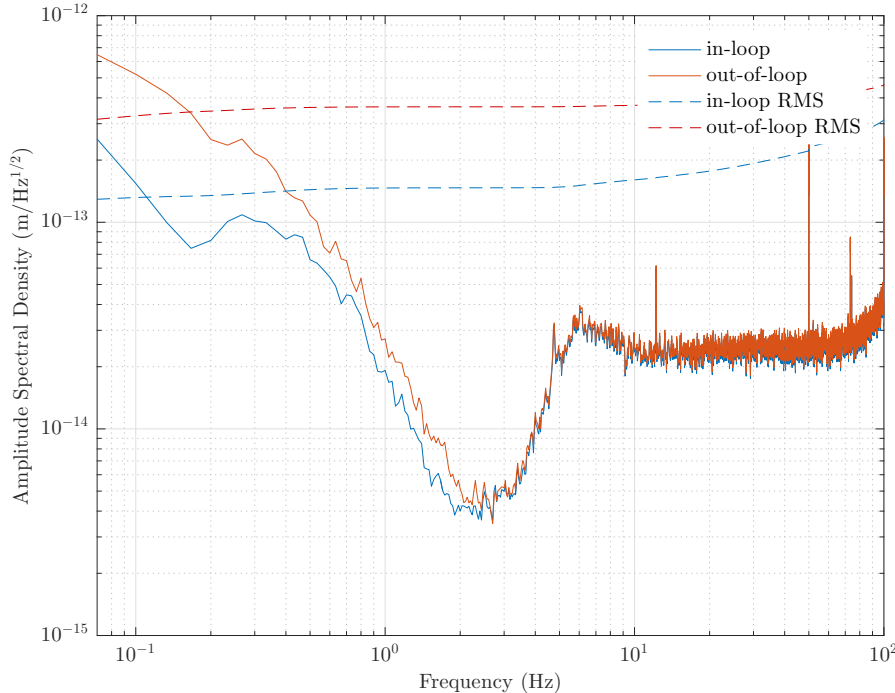


**Figure 3.** Spectra of the in-loop and out-of-loop measures of the OMC2 cavity length. The integrated low-frequency RMS of both signals are also shown. Above 5 Hz the signal is dominated by laser frequency noise, which is slightly lower than in figure 2 due to higher gain laser frequency control. Below that frequency the out-of-loop length RMS is  $3.5 \times 10^{-13}$  m.

### 5. Length control precision

The cavity length fluctuations couple to the gravitational wave detector sensitivity through (4), where the lock precision  $\Delta l_{\text{rms}}$  is a critical parameter. In section 4 we used a low gain on the OMC2 cavity length control to limit re-injecting frequency noise with the loop and to simplify the result interpretation. To improve the lock precision, the OMC is operated with a factor 10 higher loop gain and a unity gain at a few Hz. As in the previous section the loop feedback is dominated by the Peltier cells temperature feedback below 0.1 Hz and by the PZT feedback above this cross-over frequency. Figure 3 shows the OMC2 error point spectrum for a high gain loop using the in-loop and out-of-loop PD. This achieves  $\Delta l_{\text{rms}} = 3.5 \times 10^{-13}$  m for the out-of-loop signal, over 3 times lower than the design requirement [1].

In Advanced Virgo the precision of the laser lock onto the reference cavity is  $\sim 1$  Hz RMS [1], which through 6 is equivalent to  $4.4 \times 10^{-16}$  m, that is a laser frequency control orders of magnitude better than the one achieved here. Therefore in the real case the laser frequency should not be dominant as in the test setup presented here, and the OMC lock precision should be easily reproduced even with a lower control loop gain.

Using 4 we combine the achieved lock precision  $\Delta l_{\text{rms}}$  and the measured upper limit on cavity noise  $\delta l$  shown in figure 2 to obtain the expected contribution of OMC length noise to the Advanced Virgo measurement noise shown on figure 4.

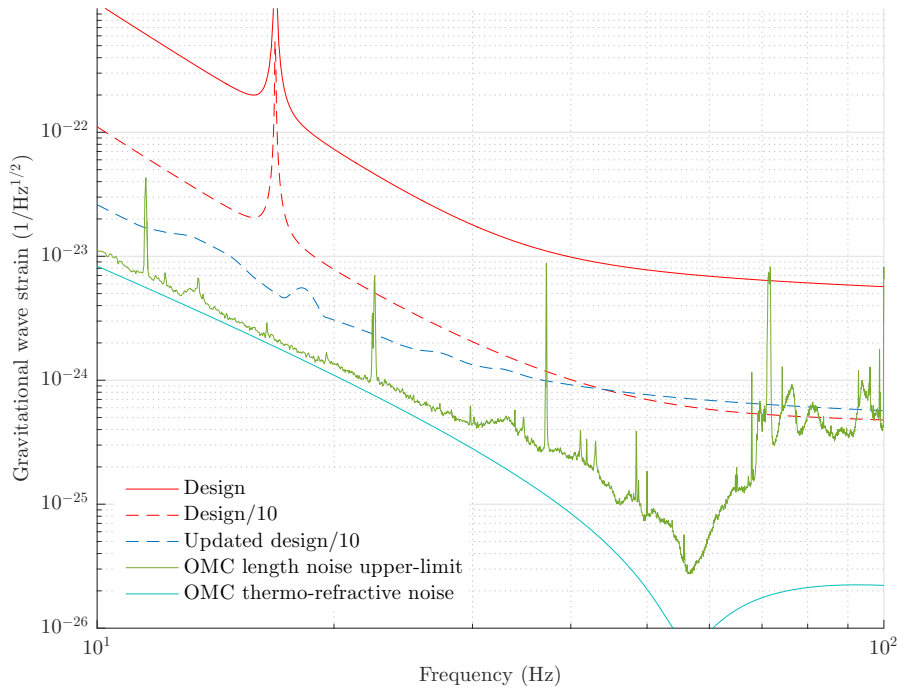


**Figure 4.** Projection of the upper-limit on OMC length noise from figure 2 onto the Advanced Virgo design noise curve assuming a lock precision of  $3.5 \times 10^{-13}$  m and a detuned signal recycling configuration. The original design and updated design Advanced Virgo noise curves are shown.

Below 60 Hz this expected broadband noise is at least 10 times smaller than the Advanced Virgo design sensitivity [10] or the updated sensitivity expectation using more accurate suspension thermal noise models [1]. Above 60 Hz the measured OMC length noise upper limit is dominated by mechanical resonance of the measurement setup, nonetheless it remains below the design sensitivity curve. In Advanced Virgo these resonances should not be present as the OMC will be placed on a suspended bench in vacuum.

The prominent lines at 11.53 Hz, 22.53 Hz and 37.23 Hz are narrow, with respective linewidths of 30 mHz, 100 mHz and 30 mHz. Hence regardless of whether these are real length noise or a sensing noise of this particular measurement, these lines will not have an impact on the broadband gravitational wave sensitivity that is relevant for most gravitational wave signals, such as coming from compact binary coalescences [16].

Note that in the initial broadband configurations [10] the constraints on the OMC length noise are  $\sim 10$  weaker than in the configuration optimized for binary neutron star detection. Indeed, without signal recycling or with signal recycling tuned the optical gain at 10 Hz is about an order of magnitude higher, hence the OMC length noise coupling in these cases is 10 times smaller at low frequency than presented here.



## 6. Conclusions

We have measured an upper limit on the Advanced Virgo OMC cavity length noise. In the 10-20 Hz band this upper limit is consistent with the thermo-refractive noise prediction, confirming that there is no other significant length noise in this cavity design.

We achieved a lock precision of  $\Delta l_{\text{rms}} = 3.5 \times 10^{-13}$  m, which is a factor 17 better than obtained previously for the Virgo OMC [10]. Combining these two results we have shown that the OMC length noise contribution to the Advanced Virgo measurement should be at least a factor 10 below other expected noise sources in the 10-60 Hz band, which is most challenging for technical noises. This gives confidence that the OMC noise should not be a limiting factor in the forthcoming Advanced Virgo observations.

The achieved gap between the expected OMC noise contribution and Advanced Virgo noise opens the prospects of further parameter optimization depending on the issues encountered during the first Advanced Virgo operations. For example the radio-frequency sideband filtering could be improved by an order of magnitude by increasing the OMC finesse by a factor 2. This would increase the thermo-refractive noise by a factor 4 but it would still remain a factor 10 below other expected noises.

## Acknowledgments

We would like to thank our Advanced Virgo collaborators for numerous discussions that lead to the design and optimization of the OMC cavities discussed here.

## References

- [1] F. Acernese et al. Advanced Virgo: a second-generation interferometric gravitational wave detector. *Class. Quantum Grav.*, 32:024001, 2015.
- [2] J. Aasi et al. Advanced LIGO. *Class. Quantum Grav.*, 32:074001, 2015.
- [3] K. L. Dooley et al. GEO 600 and the GEO-HF upgrade program: successes and challenges. *Class. Quantum Grav.*, 33:075009, 2016.
- [4] S. Hild et al. DC-readout of a signal-recycled gravitational wave detector. *Class. Quantum Grav.*, 26:055012, 2009.
- [5] T. Fricke et al. DC readout experiment in Enhanced LIGO. *Class. Quantum Grav.*, 29:065005, 2012.
- [6] K. Numata, A. Kemery, and J. Camp. Thermal-noise limit in the frequency stabilization of lasers with rigid cavities. *Phys. Rev. Lett.*, 93:250602, dec 2004.
- [7] G. Vajente and J. Marque. Controlling advanced gravitational wave detector output mode cleaners acting on the laser frequency. *Astropart. Phys.*, 41:45, 2012.
- [8] M. Prijatelj et al. The output mode cleaner of GEO 600. *Class. Quantum Grav.*, 29:055009, 2012.
- [9] F. Beauville et al. Improvement in the shot noise of a laser interferometer gravitational wave detector by means of an output mode-cleaner. *Class. Quantum Grav.*, 23:3235, 2006.
- [10] T. Accadia et al. Advanced Virgo Technical Design Report. Technical report, 2012. VIR-0128A-12.
- [11] M. Ducrot et al. Measurements of Advanced Virgo OMC cavities finesse. Technical report, 2014. VIR-0458A-14.
- [12] V. B. Braginsky and S. P. Vyatchanin. Corner reflectors and quantum-non-demolition measurements in gravitational wave antennae. *Phys. Lett. A*, 324:345, 2004.
- [13] D. Heinert, A. G. Gurkovsky, R. Nawrodt, S. P. Vyatchanin, and K. Yamamoto. Thermorefractive noise of finite-sized cylindrical test masses. *Phys. Rev. D*, 84:062001, 2011.
- [14] M. L. Gorodetsky and I. S. Grudinin. Fundamental thermal fluctuations in microspheres. *J. Opt. Soc. Am. B*, 21:697, 2004.
- [15] *Mephisto Product Line User's Manual*, 2003.

- [16] B. P. Abbott et al. Binary Black Hole Mergers in the First Advanced LIGO Observing Run. *Phys. Rev. X*, 6:041015, 2016.